Absolute Quantum Efficiency Measurements of a Prototype Ultra-Cold Neutron in Liquid Helium Detection System

by

Irfan Ahmed Siddiqi

Submitted to the Department of Physics
on May 12, 1997, in partial fulfillment of the
requirements for the degree of
Bachelor of Arts

Abstract

This study evaluates the absolute quantum efficiency of a XUV down-conversion system proposed by Doyle and Lamoreaux [2] for use in an experiment to measure the neuton beta-decay lifetime, t_b, by magnetically trapping ultra-cold neutrons (UCN). The UCN are produced (scattered) via the "superthermal" process. The detection method relies on down-converting XUV photons generated during collisions between the beta particles and the surrounding superfluid He^4 (where the UCN are stored). XUV photons are first converted into the blue by using the organic scintillator 1,1,4,4 tetraphenyl butadiene (TPB). Subsequently, the blue light is transported out of the magnetic trapping region (cell) by a wavelength shifting (WLS) fiber. Outside of the cell, the WLS fiber is coupled into a photon detection system.

A miniature cell is constructed and immersed in a helium dewar. Scintillations are produced via an alpha source. The cell is lined with TPB. A WLS fiber (Kuraray Y11 and Pol.Hi.Tech S0048-100 were tested) runs through the cell into a PMT setup in pulse counting mode. Relative measurements of the cell efficiency (CE) are made by comparing the pulse height spectra obtained with the alpha source to a situation in which a blue light source is placed in the cell. By using an integrating sphere to obtain the total output of this light source, absolute efficiency measurements are also obtained. The XUV production rate due to alpha particle collisions is determined. Finally, efficiency measurements obtained are used to predict the feasibility of this XUV detection scheme in the proposed neutron trapping experiment.

Thesis Supervisor: John M. Doyle

Title: Associate Professor of Physics

Acknowledgments

I thank God for giving me the patience and perseverance to complete this work, through times thick and thin. To my parents I will always be indebted for their continuous support and encouragement. The same is true for the rest of my family, especially my grandparents — the ones still present and the ones that have passed on. I also owe a great debt to my friends who have always shown me the sincerest of intentions in all of their actions. May God bless them all and raise their ranks.

I thank all the members of the Doyle group for helping put this thesis together. Special thanks are reserved for Daniel McKinsey for his support in all aspects of the project. James Butterworth is also to be acknowledged for his thoughtful ideas and help. To Clint Brome I owe many thanks for supplying the evaporated TPB samples placed in the experimental cell. And of course, I am appreciative of the overall guidance given by John M. Doyle.

Contents

List of Figures

List of Tables

Chapter 1
Introduction

1.1 Neutron Lifetime Measurement

The neutron lifetime t_b is a fundamental physical constant which (together with other measurements) provides a means of verifying the electro-weak theory and the Standard Model. One way this can be achieved is by using t_b in conjunction with the neutron beta-decay asymmetry coefficient (A) to determine the values of g_a and g_v, the fundamental weak force coupling constants. Comparisons can then be made between the vector coupling constant $g_{v,}$ and the first element of the Cabbibo-Kobayashi-Maskawa (CKM) mixing matrix. This matrix element, $|V_{ud}|$, can also be determined using higher generation decay data and assuming the unitarity of the CKM matrix. Turningthis around, the unitarity of the CKM matrix can be tested. Measuring the neutron lifetime thus is an important component of a direct test of the Standard Model. Other important uses for t_b are found in cosmology, particularly in the theory of nucleosynthesis [1].

Recent experiments aimed at obtaining the neutron beta decay lifetime have produced results with uncertainties ranging from 0.2-1%. Although this accuracy is sufficient for many applications, valuable insight into many physical processes can be gained through higher accuracy measurements. For example, measurements for $|V_{ud}|$ derived from purely leptonic muon decay are in reasonable agreement with those obtained from unitarity arguments. However, determination based on current neutron lifetime data are discrepant. To ascertain whether this discrepancy lies in the inaccuracy of t_b or is indicative of physical effects beyond the Standard Model, further measurements of the neutron lifetime are required. Accurate measurements of t_b also allow for the calculation of the pp and pep reaction matrix elements which predict the nuclear processes in stellar cores. Additionally, values of the universal baryon density W_b can be determined and used to provide a check on the Big Bang Nucleosynthesis theory [1].

Doyle and Lamoreaux [2] have proposed to improve the current uncertainty in t_b by a factor of 100 through the use of magnetically trapped ultra-cold neutrons (UCN). This method utilizes the magnetic interaction of the neutron (magnetic moment = 0.7 mK/T) with a magnetic field gradient. Low-field-seekers settle in regions where the applied field is a minimum. The trap can be loaded by via producing (scattering) UCN using the "superthermal" process which relies on the phonon interactions between neutrons and superfluid He^4. Once trapped, the UCN undergo decay and emit beta particles into the surrounding helium. These beta particles subsequently cause the helium to scintillate in the

XUV range (50-100nm). By detecting these scintillations, it is then possible to count neutron decay events versus time and thus infer the neutron lifetime.

1.2 XUV Detection

A crucial component of this method is the detection of the XUV photons generated in the magnetic trap by UCN undergoing beta-decay. The proposed detection scheme consists of first down-converting the XUV photons into the visible range by using the organic scintillator 1,1,4,4 tetraphenyl butadiene (TPB). This compound absorbs an ultraviolet photon and emits a blue photon with an emission maximum of 440 nm [3]. The scintillator is coated on the inside of a cylindrical cell which encompasses the trap region. The 440nm light is allowed to travel into a wavelength-shifting-fiber (WLS). The fiber absorbs the blue light and emits in either another region of the blue or in the green, depending on the particular fiber used. By coupling the fiber into a photon counting system, the light from the WLS fiber is detected.

In order to assure that the beta-decay events are detectable, it is necessary to determine the losses due to the various components used in the chain of conversions and transmissions that are part of the detection apparatus. The work presented here focuses on evaluating the absolute quantum efficiency of the proposed detection scheme in a small experimental cell which is similar in geometry and functionality to the one developed in the Doyle Group, but is only a fraction of its size. Though the efficiency measurements obtained in this experiment are significantly influenced by the geometry of the setup, they are nevertheless valuable in characterizing the loss processes present, and ultimately in predicting the behavior of the larger cell that will actually be used in the neutron experiment.

Chapter 2
Experimental Setup

2.1 Overview

The overall setup of this experiment is comprised of two basic parts: the cryogenic apparatus and the calibration apparatus. Consisting of the experimental cell and the cryogenic probe, the cryogenic apparatus is designed to simulate an environment in which XUV photons are produced and detected via the scheme described in the previous section (1.2). Inside the cell the XUV photons are generated and converted into the visible. The experimental cell is cylindrical in shape with TPB on the inside surface. By inserting the cell into the cryogenic probe (the probe simply being a plastic tube), it is possible to lower it into a liquid helium storage dewar (see figure 1). Beta-decay scintillations within the liquid helium are mimicked by way of a radioactive alpha source. An alpha source was used instead of a beta source in these experiments due to availability of sources in the lab. The source is fixed to a stainless steel rod and is inserted into the cell.

The cell is the part of the apparatus that is surrounded by scintillation. Down-converted by the organic scintillator layer, XUV photons are converted into blue photons and are subsequently captured by a WLS fiber. Since both Gortex and TPB are optically reflective, a large proportion of blue photons that are not absorbed by the fiber upon initial emission by the TPB undergo reflections and are eventually captured. The WLS fiber passes through the cell and exits the cryogenic probe where it is coupled into a photomultiplier tube (PMT).

One of the goals of this work is to determine how well blue light (peak emission 440 nm) can be transported from inside the cell to the photodetector. Because the florescence efficiency (FE) of TPB has already been determined [4], the performance of the blue light transportation system is of great importance in evaluating the overall characteristics of this XUV detection system.

Measurements taken from the cryogenic apparatus are relative. The number of XUV photons being produced cannot be determined directly since there is a large uncertainty

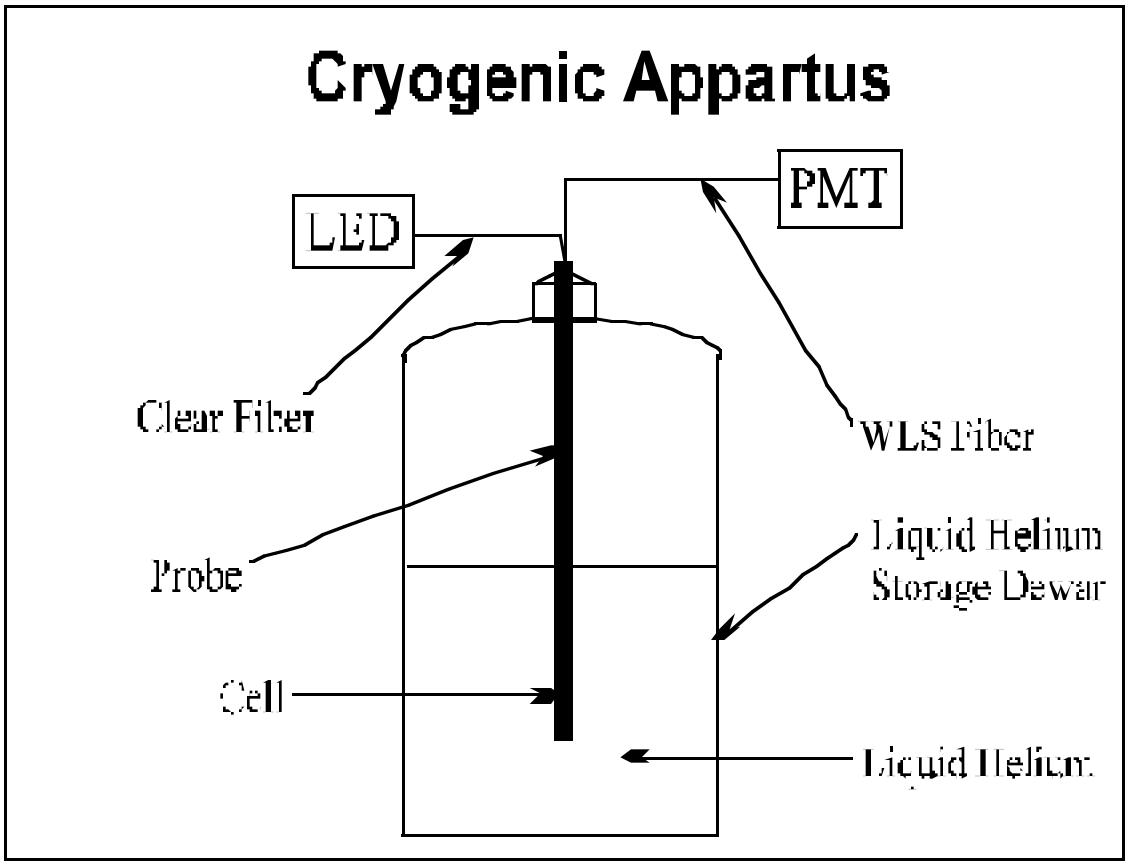

Figure 1: Cryogenic Apparatus

associated with both the total decay rate of the source and the number of XUV photons released during a single alpha-helium collision. As a result, the number of photons exiting when XUV down-conversion is taking place is compared to the signal observed when a pulsed blue light source is placed in the cell. A small, spherical Teflon diffuser is located within the cell and is used (along with a light emitting diode) to provide this source of light. This blue light is generated by a high brightness light emitting diode (LED) and is transported down into the diffuser using a clear optical fiber.

The calibration apparatus allows the relative measurements (made with the cryogenic apparatus) to be converted into absolute ones. The calibration setup is used to determine the total number of blue photons emitted by the Teflon diffuser in each pulse. This is accomplished by placing the Teflon diffuser into an integrating sphere. A photodetector is coupled into the exit port of the integrating sphere. By knowing the number of blue photons present in the cell with the diffuser in place and the number detected outside the cell, a ratio called the transport efficiency, TE, is obtained.

It is then possible to calculate the number of blue photons being emitted from the

TPB when the alpha particles are inducing XUV scintillations. This measurement is in turn, then used in conjunction with the florescence FE of TPB, to determine the number of XUV photons being generated. With these values, the system performance can be evaluated since the number of visible photons observed and XUV photons generated in the liquid helium is known. By estimating the decay rate of the radioactive source, the number of XUV photons produced per unit energy can be determined. Similar measurements exist for XUV scintillations in liquid helium when the incident particles are electrons [19].

In sections 2.2- 2.4, the various parts of the cryogenic and calibration apparatuses are described in detail. Given under the heading of cryogenic apparatus (section 2.2) are all the individual components of the cell and probe. The major components of the calibration apparatus are the integrating sphere (see section 2.4) and the photodetector. The same photodetector is used in both the cryogenic and calibration setup (see section 2.3).

2.2 Cryogenic Apparatus

2.2.1 Experimental Cell and Cryogenic Probe

In this section the materials used to construct the experimental cell and the cryogenic probe as well as the principle features of their design are discussed. The functional components of the cell — TPB layer, WLS fiber, radioactive source, and diffuser — and probe are discussed in sections 2.2.2-2.2.5. Figure 2 details the experimental cell used in the making the initial, relative measurements.

The cell is constructed of thin-walled stainless steel tubing 0.90”od and 4.25” long. Inside the outer cylinder there is another cylinder which is of the same length but of diameter 0.75”. This type of cylinder within a cylinder construction is used to allow the actual cell to have both a small diameter and to be mounted within the cryogenic probe, whose inner diameter is one inch. Having a small cell diameter increases the fraction of blue light incident on and thus transported by the WLS fiber. At the same time, however,

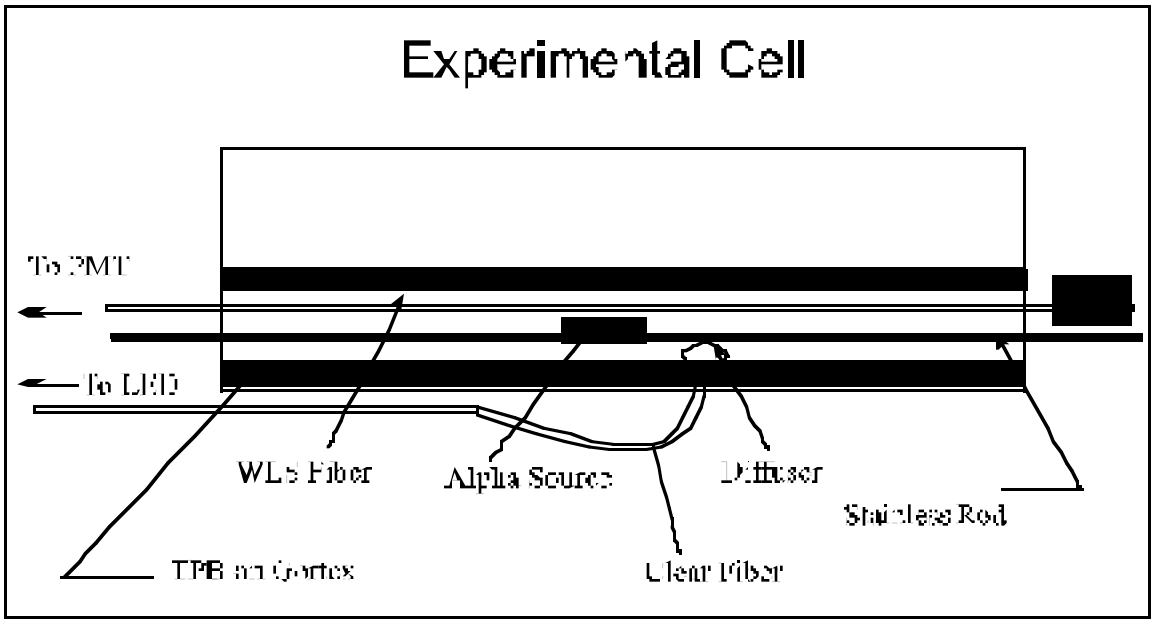

Figure 2: Experimetnal Cell

it is useful to have a relatively large cryogenic probe so that the optical fibers being fed into the cell do not have to be forced into small radius turns, preventing cracking and significant associated light loss. In order to minimize helium loss upon cooling, the inner cylinder is also constructed of thin-walled stainless.

The cell is slipped into the lower end of the cryogenic probe and is held in place via a screw which goes through the outer wall of the probe into the outer steel cylinder of the cell. Constructed of Garolite "G10" [6], a very low thermal conductivity plastic resin which is frequently used in cryogenic applications, the probe is painted black with Stycast 2850 epoxy [7] to prevent light transmission, and is approximately 39" in length (see figure 3). At the top of the probe is an aluminum cap which has a compression ring grove machined into it so as to allow the entire setup to be immersed into a liquid helium storage dewar. The aluminum cap is machined to the specifications of the actual storage dewar cap, thus allowing the same sealing clamps to be used to prevent any excess helium boil off. At the bottom of the cryogenic probe is an aluminum disc with various holes machines into it (see figure 4). It is through these holes and the holes in the top aluminum cap that the WLS fiber and alpha source rod are held in place.

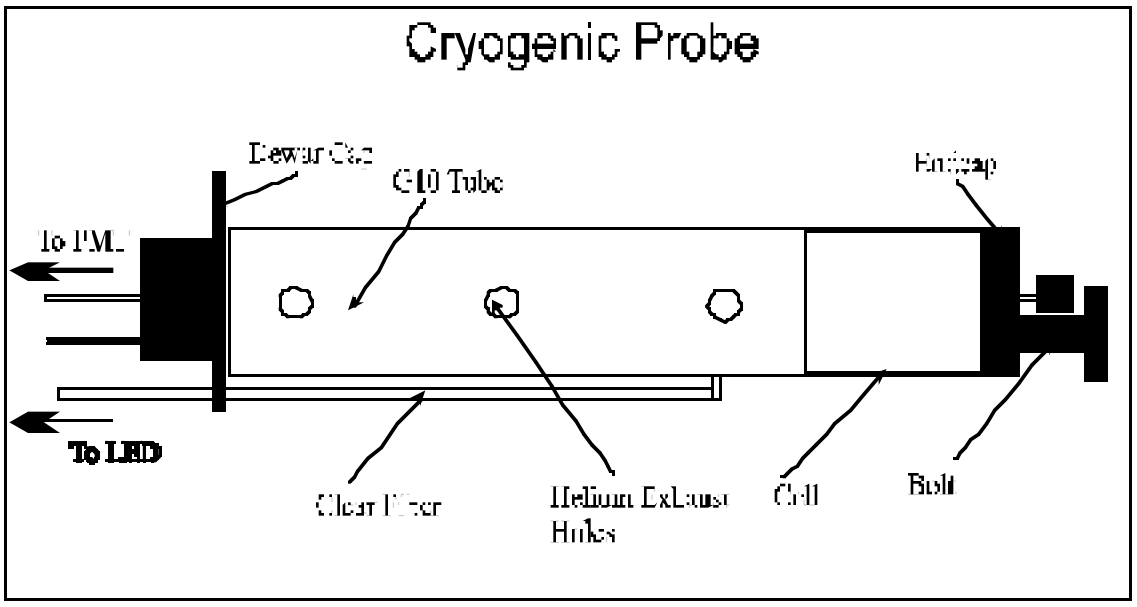

Figure 3: Cryogenic Probe

2.2.2 TPB Layer

Inside the inner cell, a sheet of Gortex (0.125" thick) coated with evaporated TPB is rolled up and snugly fit. The TPB is evaporated onto the Gortex using a Varian evaporator. The typical evaporator current used was 60A. The TPB thickness is estimated to be 0.2 +/- 0.1 mg/cm^2.

TPB is one member of a class of organic compounds called conjugated dienes. In these systems, the energy gap between the bonding and anti-bonding pi orbitals is reduced through hyperconjugation. As a result, a TPB molecule is able to accept a XUV photon and promote an electron into a higher energy pi orbital. When this electron relaxes, light in the blue wavelength regime is emitted. The emission spectrum is measured by [3] to be peaked at 440nm with an approximately 70nm full width at half maximum (FWHM) (see figure 5a). The fluorescence efficiency of TPB is defined as the ratio of blue photons emitted to XUV photons absorbed. Recent studies have shown the relative fluorescence efficiency of evaporated TPB films, up to thicknesses of approximately 1mg/cm^2, to be 3.9 times that of evaporated sodium salicylate for a 58.4 nm input and 3.7 for a 74.0 nm input [4] (see figure 5b). Bruner [5] has measured the absolute quantum efficiency of

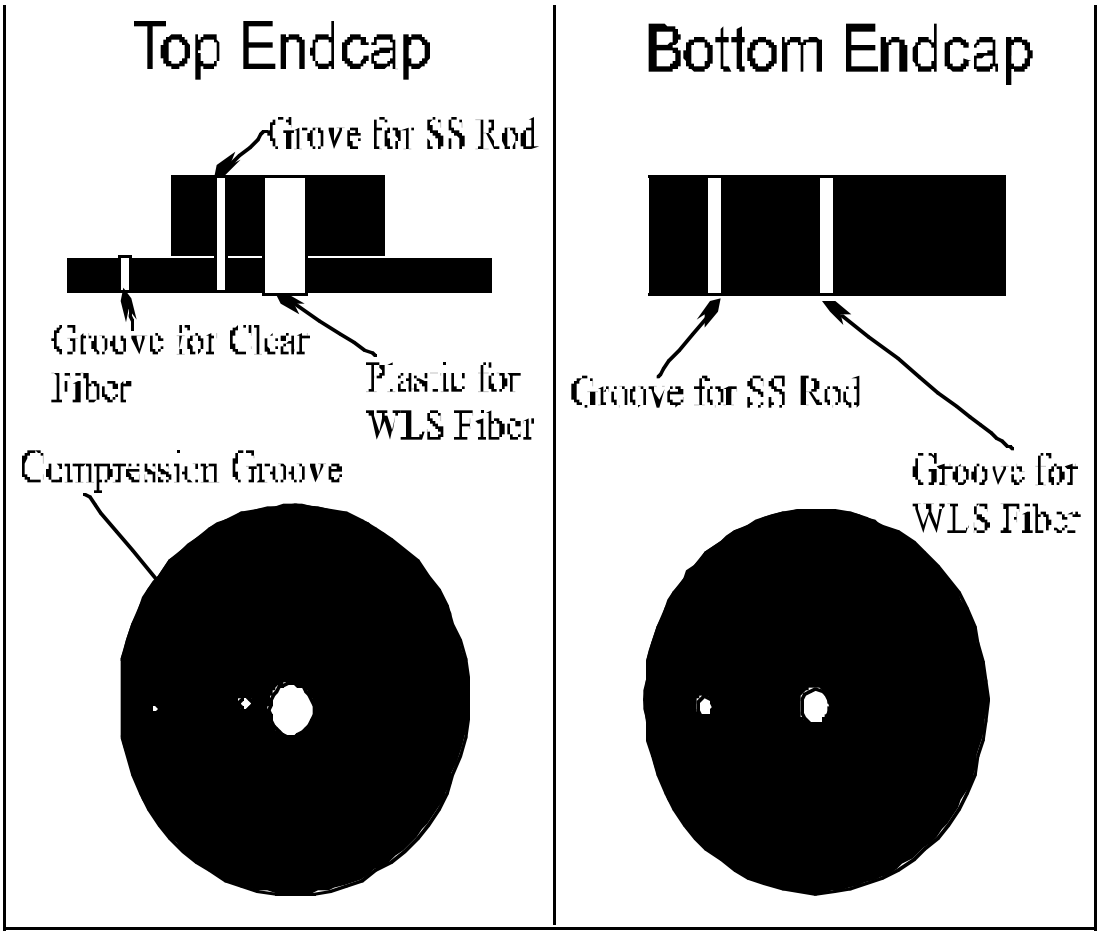

Figure 4: Cryogenic Probe Endcaps

evaporated sodium salicylate to be 42% for a 58.4 nm excitation and 37% for a 74.0 nm excitation. It is thus reasonable to approximate that the TPB coating inside the experimental cell will have an absolute fluorescence efficiency of 100%. Before running the experiment, the coating was testing using a portable soft ultraviolet lamp to make sure that there were no large imperfections in the scintillator coating.

2.2.3 WLS Fiber

The WLS fiber is secured at the top of probe by the use of a catalytic polystyrene casting resin [8]. During construction, the fiber is clamped into place while the resin is poured into the cavity in the cap and allowed to set. Since the surface of the fiber is very smooth, the viscous plastic resin does not bond to it, thus allowing the fiber to be tightly held yet removable. The fiber goes through the cell and out the bottom aluminum end cap. Once the fiber is secured at the top end, it is pulled taught and wrapped with black

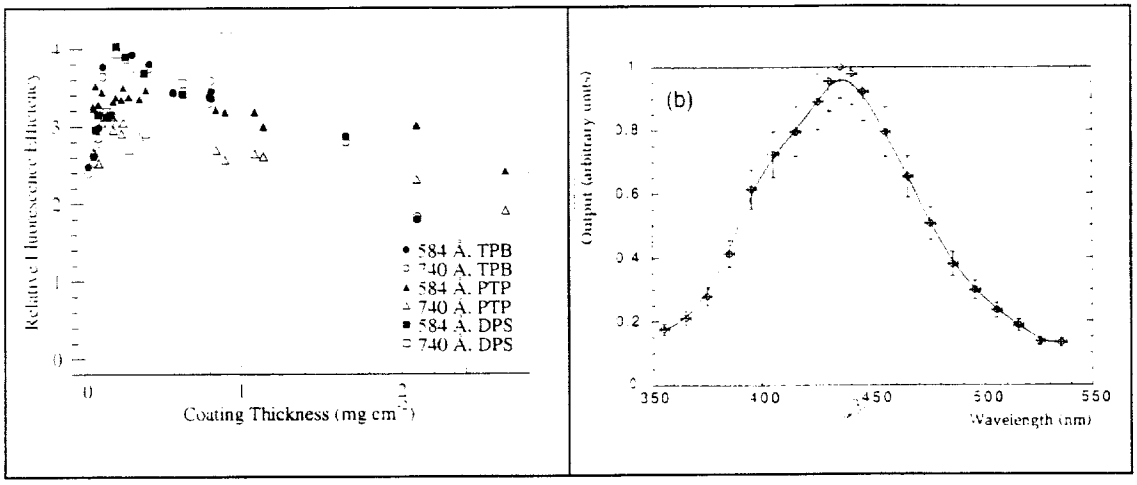

Figure 5: a) Emission Spectrum for TPB b) Fluorescence Efficiency for TPB

electrical tape at the bottom, preventing light from being reflected up the fiber from the lower end and preventing it from slipping up into the cell.

Two different fibers were used in separate runs of this experiment. In the first run, a Pol.Hi.Tech S0048-100 (hereafter S48) scintillating fiber which absorbs around 400nm and emits at 480nm [9] was used. Next, the experiment was conducted using a Kuraray Y11 150ppm fiber (hereafter Y11) which absorbs in the blue and emits around 505 nm [10]. The attenuation length of both of these fibers is estimated to be around 4.5 +/- 0.5 m [11]. Though the exact absorption and emission characteristics were not measured in this experiment, curves obtained from [12], given in figure 6, show the behavior of another typical fluor, G2.

2.2.4 Alpha Source

Similar to the WLS fiber, the stainless steel rod containing the radioactive source in also held in position by fasteners at the top and bottom of the cryogenic probe. The source is a Po^{210} alpha source (negligible gamma, 10^{-5} of decays) with a half life of 138 days. Prior to conducting this experiment, the source was measured as having an output of 3000 counts/second just before its arrival at the Doyle Group Lab [13]. The source is plated on a thin copper wire which is soldered onto a 1/32" diameter stainless still rod. The rod runs through the cell and its ends protrude out from the top and bottom of the cryogenic probe. At the bottom end, a 1/2" stainless steel bolt is attached to the rod via stainless lock wire. An alligator clip is placed at the top of the probe to prevent the rod from falling into the probe. When it is required to move the alpha source into or out of the cell, the clip is removed and

the rod is positioned appropriately. This system relies simply on gravity to allow unrestricted movement; a great convenience since pulleys and other mechanical devices often exhibit erratic performance at 4.2K.

2.2.5 Teflon Diffuser

The last structural component of the cryogenic setup is the Teflon diffuser. A _" diameter Teflon sphere is used. Bringing blue light into the sphere is a clear plastic, optical grade fiber. The fiber is unjacketed and is 1mm in diameter. A high refractive index material, polymethyl-methacrylate, comprises the core of the fiber, and a low index fluorine based polymer is coated on the outside. With an attenuation of only on the order of 350 dB/km in the blue [14], this fiber ensures that blue light is efficiently transported into the diffuser. A high illumination LED [15], typical output ~1200 mcd, is coupled to

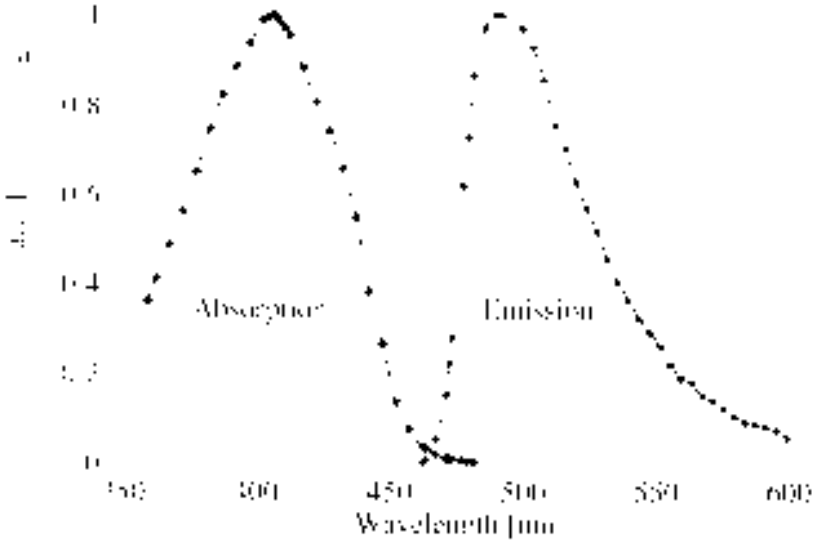

Figure 6: Absorption and Emission Spectra for G2

the clear fiber, which runs along on the outside of the cryogenic probe up through the top of the aluminum cap. The fiber is coupled to the LED through a 1" Teflon cube which has holes of diameter 1mm and 5mm (see figure 7). With each component tightly held in

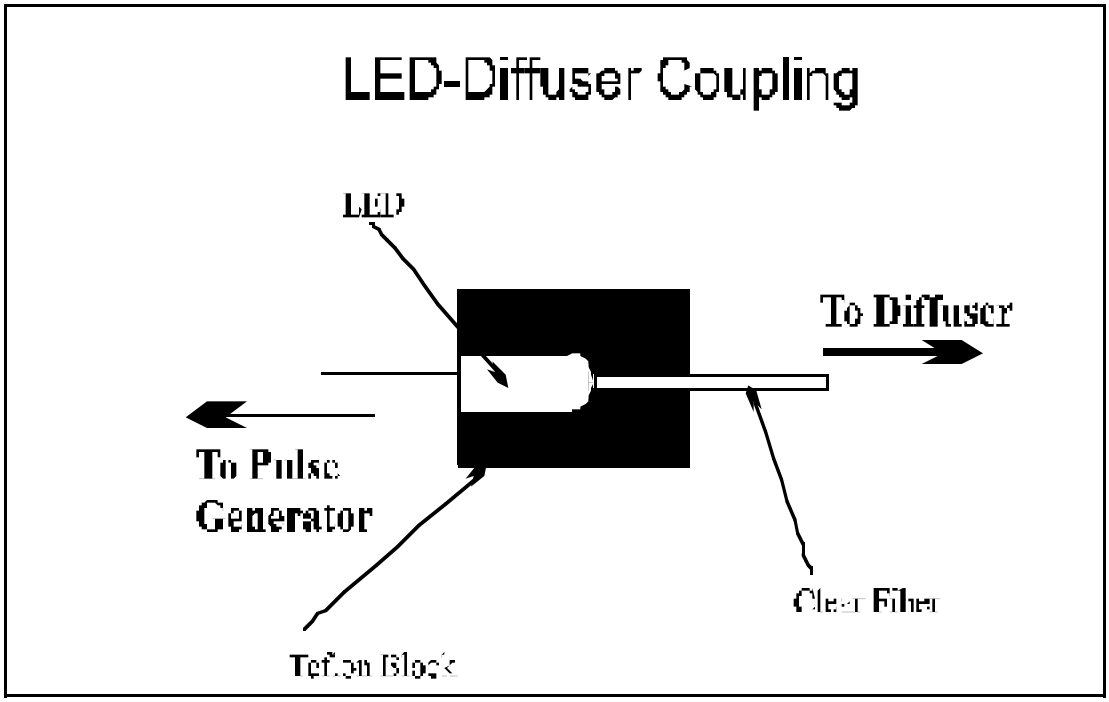

Figure 7: LED-Diffuser Coupling

place in its cavity, the fiber is made to butt up against the LED . The entire cube is taped up to securely fix both components. A 52.3 Ohm resistor is placed in series with the LED. Powering the diode is a HP 8013B pulse generator.

2.3 Photodetector Setup

In order to detect the light transported from the cell via the WLS fiber, a Burle 8575 bi-alkalai photomultiplier tube is employed (see figure 8 for block diagram), typical gain of 10^7 [16]. The PMT housing [17] is cooled using an electronic peltier cooler to reduce the dark counts. In order to stop the fiber from vibrating (and thus inducing high amplitude fluctuations in the observed light signal), it is passed through a black plastic plug which is placed into a hole in the PMT housing. The pulses arriving at the PMT anode are first directed into a Canberra 2005 Scintillation Detector Preamplifier which converts the ionization charge developed in the PMT into an exponentially decaying pulse. The amplitude of these pulses is proportional to the total charge accumulated during a particular pulse arrival. After leaving the preamplifier, the pulses are processed by a discriminator which rejects pulses with amplitudes below the lower level discriminator (LLD) level and above the upper level discriminator (ULD) level. This procedure reduces the noise pulses generated by thermionic emission and cosmic ray absorption. The LLD was set 50 mV and the ULD at 8.00 V, based on typical values for noise pulses. Pulses successfully passing through the discriminator are amplified using a Canberra 2015a Amplifier/TSCA. With the

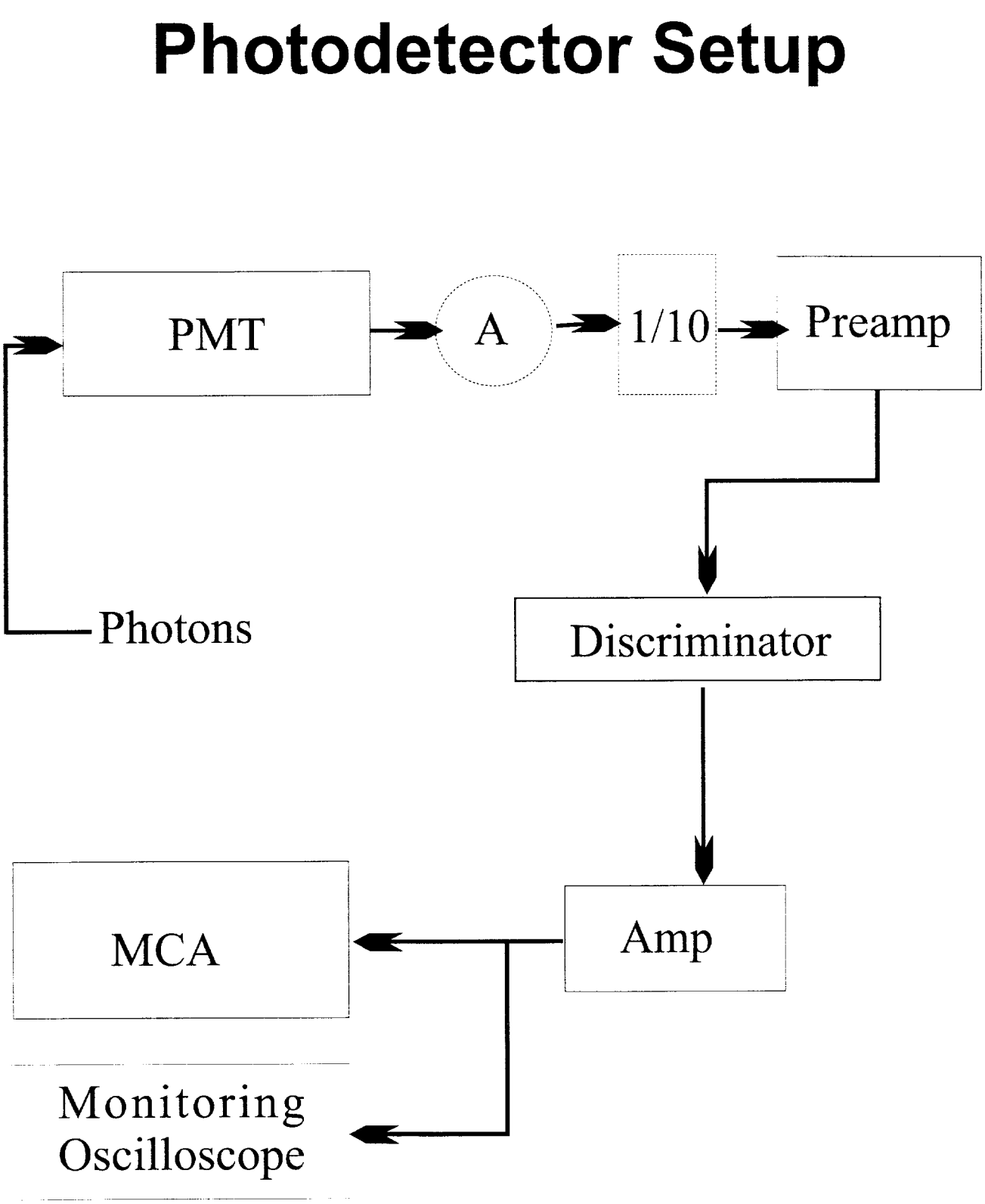

Figure 8: Photodetector Block Diagram

amplifier gain set to 4, the pulses are then sent to an Oxford PCA-P multichannel analyzer (MCA) running in ADC mode (ie. no gain is applied to the input). Using the MCA, pulse height spectra are obtained. The spectra generated by the MCA are plots of counts versus channel number. Each channel number corresponds to a particular voltage or pulse height. A calibration procedure is carried out to convert channel number into absolute units.

2.4 Calibration Apparatus

The light output of the Teflon diffuser is characterized for two important reasons. First, it is necessary to determine the total radiation emitted to obtain absolute measurements on the efficiency of the complete XUV detection cell. Secondly generating,

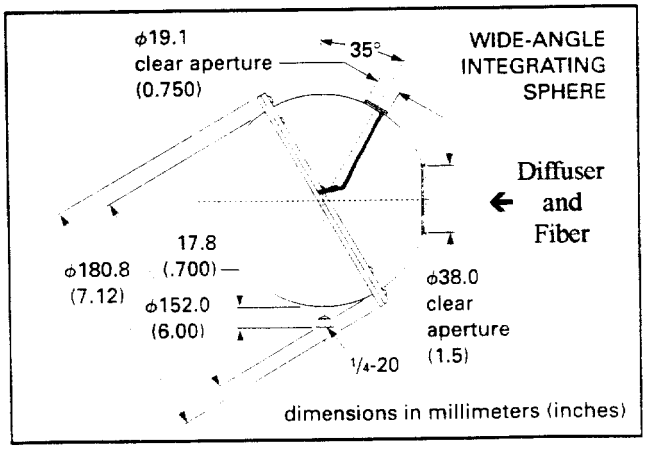

Figure 9: Integrating Sphere Setup

high luminosity pulses allows for determining the number of channels that correspond to a photoelectron. This calculation is discussed in section V.

In order to measure the total output of the diffuser, a Melles-Griot 152 mm integrating sphere is employed (see figure 9). Utilizing a highly reflective magnesium oxide coating, the sphere is able to transmit a certain percentage of the total light input onto the exit port. By calculating the throughput of the sphere, which is a function of the input and output port sizes as well as the reflectivity, it is possible to calculate what fraction of the light is exiting the sphere. The exit port of the integration sphere is directly coupled to the PMT described above. The signal processing setup, as depicted in figure 6, is employed with the only difference being that the light source is the integrating sphere and not the WLS fiber.

The Teflon diffuser is kept roughly in the center of the integrating sphere. This is

accomplished by putting a patch of Gortex wrapped with highly reflective Teflon tape over the entrance port and passing the optical fiber through an incision made in it. In order to mechanically secure the structure, black electrical tape is used to restrict movement of the diffuser within the sphere. The LED is pulsed with a pulse width of 1 microsecond, pulse height of 7.78 V, and pulse frequency of 1 kHz. When the PMT output saturated the amplifier as observed on a monitoring oscilloscope, a 1/10 voltage divider was placed before the preamplifier stage.

Chapter 3
Experimental Procedure

3.1 Calibrating the Teflon Diffuser

The first step in the entire experiment was characterizing the output of the Teflon diffuser. In this section, the procedure used to measure the total luminescent output of the Teflon diffuser is detailed. The major steps involved in this part of the experiment are related to PMT operation. Light leak detection procedures are given here. In addition, the various techniques that were used to ensure proper operation of the electronics in the photon counting setup are described.

After securing the diffuser in the integrating sphere as discussed in section 2.4, the average current output of the PMT was monitored as the PMT voltage was increased. Any light leaks present were sealed using black electrical tape. When the anode current dropped below 0.09 microamps at 2500V (and was therefore undetectable with a simple multimeter), further leak detection was carried out with the aid of the MCA (the PMT operating in pulse counting mode). This procedure yielded a dark count rate at 1500V of about 40 +/- 6 Hz, which was reduced to about 10 +/- 2 Hz by covering the PMT/integrating sphere rig with a black cloth and by minimizing the ambient light present. Because the signal/noise ratio was fairly large in this part of this experiment, the dark counts were not very significant, and hence it was not necessary to leave the cooled PMT running for some hours prior to taking data.

Before commencing data acquisition, however, the average current output of the PMT was monitored for various diffuser intensity settings in order to ensure that the average current did not exceed 10 microamps. Exceeding this current might have resulted in non-linear operation of the PMT as well as permanent damage to the photocathode. At 2500V, 1 kHz pulses 1.5 microseconds wide and 7.78 V in amplitude evoked a response of under 2 microamps, well within the safe operating parameters of the PMT. These pulse parameters represented the upper limits to be studied since 7.78 V was the maximum output of the signal generator and pulses longer in duration that 1.5 microseconds would probably be either undetectable by the MCA or unsuitable for clean LED performance since after-pulsing would set in. In fact, after-pulsing was observed for widths greater than 1.3 microseconds at an amplitude of 7.78V. Narrow spikes accompanying Gaussian peaks in the pulse height spectrum were taken to be indications of non-ideal LED performance. To avoid any of these effects, pulse widths of 1.0 microseconds were used. At this pulse width, a pulse amplitude of 7.78V was sufficient to saturate the amplifier, and required

that a 1/10 voltage divider be placed before sending the PMT output to the preamplifier. Saturation was observed when the pulses emitted by the amplifier were no longer sharply peaked. Anticipating that a large fraction of the light emitted by the diffuser would not be observed when placed in the actual cell, placing a voltage divider was preferred to simply lowering the LED voltage as the latter would reduce the diffuser light output.

Once the amplifier output was deemed suitable in terms of pulse shape, the signal generator output and the amplifier output were observed using a single oscilloscope to assess the transient response of the setup shape (see figure 10 for output). Characteristic rise and fall times were less than a microsecond, thus posing no possibility of pulse overlap at a 1kHz generator frequency. Having thoroughly inspected the amplifier output, 1 minute pulse height spectra were generated for a fixed setting of the signal generator. Since the high brightness LED was operated at a fairly high voltage with only a 52.3 Ohm series resistance, the diffuser was relatively bright and the pulses observed generated a multiple photoelectron peak. In this regime, the pulse height spectrum was assumed to be Gaussian. By applying the statistical properties of a Gaussian, the number of photoelectrons corresponding to the observed data was calculated. This information was valuable since it, when used in conjunction with the integrating sphere throughout and PMT quantum efficiency, yielded the photons present in each light pulse. In addition, the conversion between ADC channel number and photoelectron number, a constant characteristic of a given PMT voltage and amplifier gain, was established. This conversion factor was used in later stages to study less intense signals where determining the number of photoelectrons corresponding to an observed peak became difficult.

Two tests were performed to determine whether the method of calculating the ratio between channel number and photoelectron count was valid. First, as the spectra given in the section 4.1 illustrate, the PMT voltage was varied while the incident light intensity was held constant. Analyzing the spectra on the basis of pulse characteristics yielded reasonably close values for the number of observed photoelectrons. This was taken to be an excellent indication of the validity of the applied method. Second, the effects of the 1/10 voltage divider were studied prior to its use. For a given PMT voltage and incident light level, spectra were taken with and without the 1/10 divider in place. In these spectra, the channel number corresponding to the pulse maximum shifted by 10, without any noticeable offset. In addition, the calculated number of photoelectrons was in reasonable agreement for both configurations.

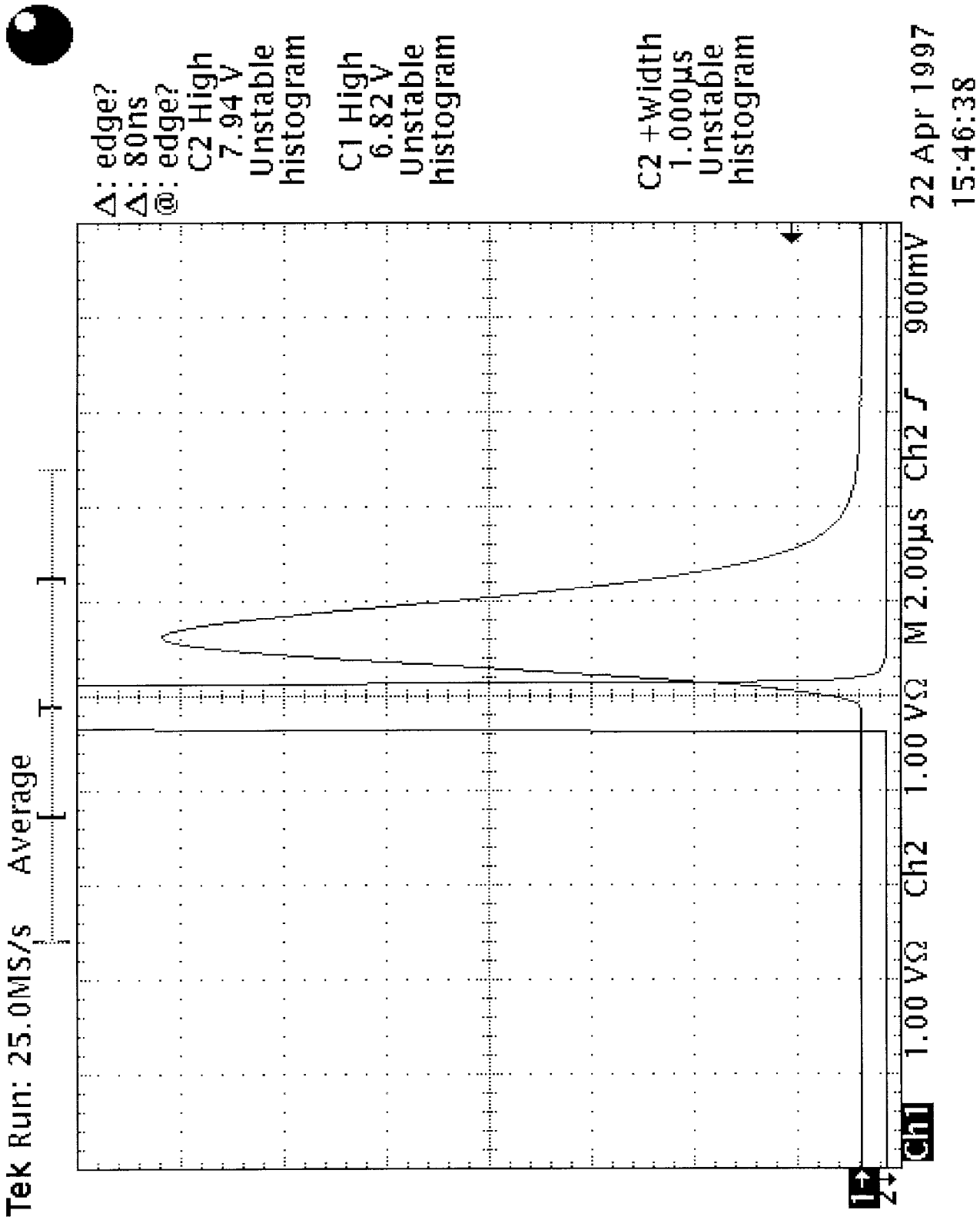

Figure 10: Square Wave Pulse Generator Output
Amplifier Output

3.2 Loading the Cryogenic Apparatus

In this section, the procedures involved in the second phase of the experiment are described. Detailed here are the techniques used in preparing the experimental cell and cryogenic probe for data acquisition. Specifically, methods for reducing XUV photon loss and ensuring signal integrity are discussed. Also described here are the specifics involved in PMT operation for this part of the experiment.

In order to minimize XUV photon loss, excess moisture was removed from the cell before taking any data. This was accomplished by either letting the cell dry out at room temperature over night or through the use of a heat gun set on very low heat for 30 minutes, if it was necessary to remove the probe from the liquid helium before the completion of a run. Having dried the cell, the WLS fiber and alpha source were loaded into the probe along with the stainless steel double cylinder cell. Measurements were made to determine how much to raise and lower the alpha source to ensure its proper positioning. After tightening all the endcaps, the cell was lowered into a liquid helium storage dewar. Holes in the upper section of the probe allowed the gas boiling off to escape as liquid filled the inner chambers. Having cooled down, light leaks were minimized using the procedure outlined in section 3.1.

In order to reduce the dark counts, the PMT was allowed to run at high voltage for 3-4 hours before taking and data readings. This reduced the noise down to 3 +/- 1 Hz at 1500V. Pulse height spectra one minute in duration were subsequently generated for (separately) the alpha source removed (background), the alpha source in place, and the Teflon diffuser switched on. As a check on the signal being observed, the PMT voltage was modulated from 1500-2500V and the signal behavior was studied. The 1/10 voltage divider was removed for these runs as the light levels being observed were relatively low. By analyzing the pulse height spectra, the efficiencies of various elements of the XUV detection system, as arranged in this particular geometry were calculated.

Initially, the experiment was conducted using the PMT in current mode. The LED was biased with a continuous current, and an average PMT current was recorded for the integration sphere output using a simple ammeter. This procedure had to be abandoned when data acquisition in the experimental cell was attempted since the signal produced with the alpha source in place was too small to be detected with the PMT in current mode. At this point, the photodetection setup was modified to the form described in section 2.3, with the PMT rigged for pulse counting.

While acquiring data with the alpha source in the cell, steps were taken to ensure that the signal observed was independent of small perturbations in the position of the alpha source. At 1900V, spectra were taken three times for each fiber and the total number of

counts was compared. In each of these runs, there was little variation of the count integral and it was then inferred that the signal observed was not some accident resulting from a particular orientation of the source. For example, if the source had been in contact with the WLS fiber, there is a possibility that it could scintillate directly into the fiber.

In addition to moving the source at a constant PMT voltage, the opposite procedure was performed as well. With the alpha source in a fixed position, the PMT voltage was raised up to 2500V. The net count integral (observed counts - background) did not change. The pulse shape did change as expected due to gain effects. This procedure provided a second method of verifying that the signal being observed was really due to the scintillations in the liquid helium.

Chapter 4
Data

4.1 Teflon Diffuser Output

Given in figure 11 are the pulse height spectra obtained from the integrating sphere setup described in section 2.5. Essentially a measure of pulse height, the horizontal axis on the raw spectra was measured in the arbitrary units of "channel number." The channel numbers on the ADC range from 1-1024. The spectra given here are plots of counts vs. photoelectron number. The procedure used is carrying out this transformation is crucial to the data analysis and is discussed in detail in chapter 5. Since the channel number is not physically relevant by itself, spectra are only given in photonelectron number. Background spectra were taken, but their amplitudes were so small as to be negligible because of high signal amplitude in these runs.

Similar to the spectra described in the previous section, the spectra given in figures 12 and 13 are again in units of counts vs. photoelectrons. These spectra are for the signal observed for the Teflon diffuser when placed in the cryogenic rig. One set of spectra is for the Y11 Fiber and one for the S48. In this instance, as expected, the light levels detected were lower and background counts were not insignificant. For each run, a background spectrum is given for comparison. The data given has the background subtracted.

4.2 Scintillation Data

Given in figures 14 and 15 are the pulse height spectra when placing the alpha source into the middle of the experimental cell. Like the spectra in figures 9 and 10, the background counts have been given and the data shown has the background already subtracted. In these runs, the one photoelectron peaks are not visible and the net integrals were recorded for these runs as being 29,400 for the Y11 fiber and 64,400 for the S48 fiber.

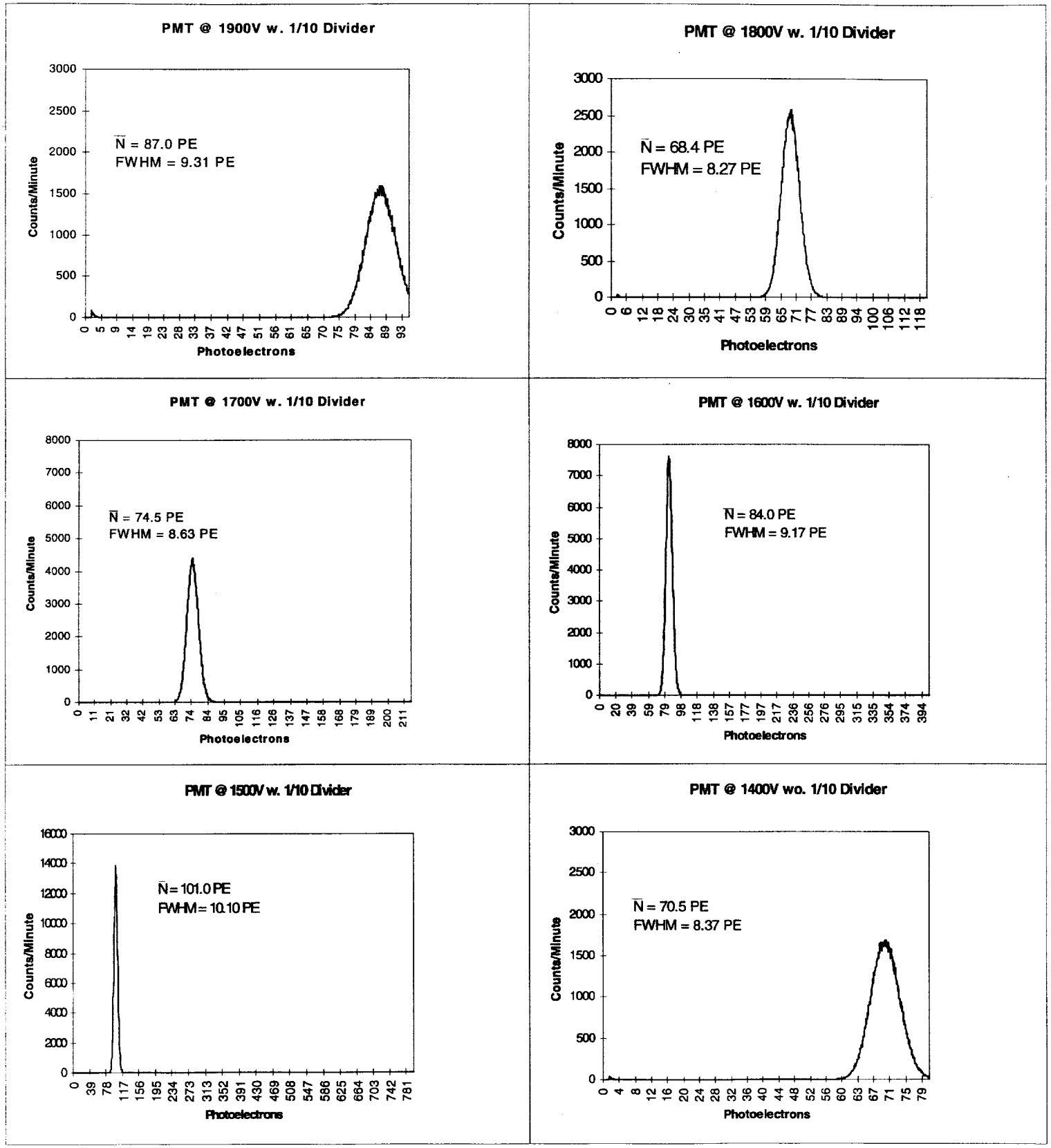

Figure 11: Pulse Height Spectra for the Teflon Diffuser in the Integrating Sphere

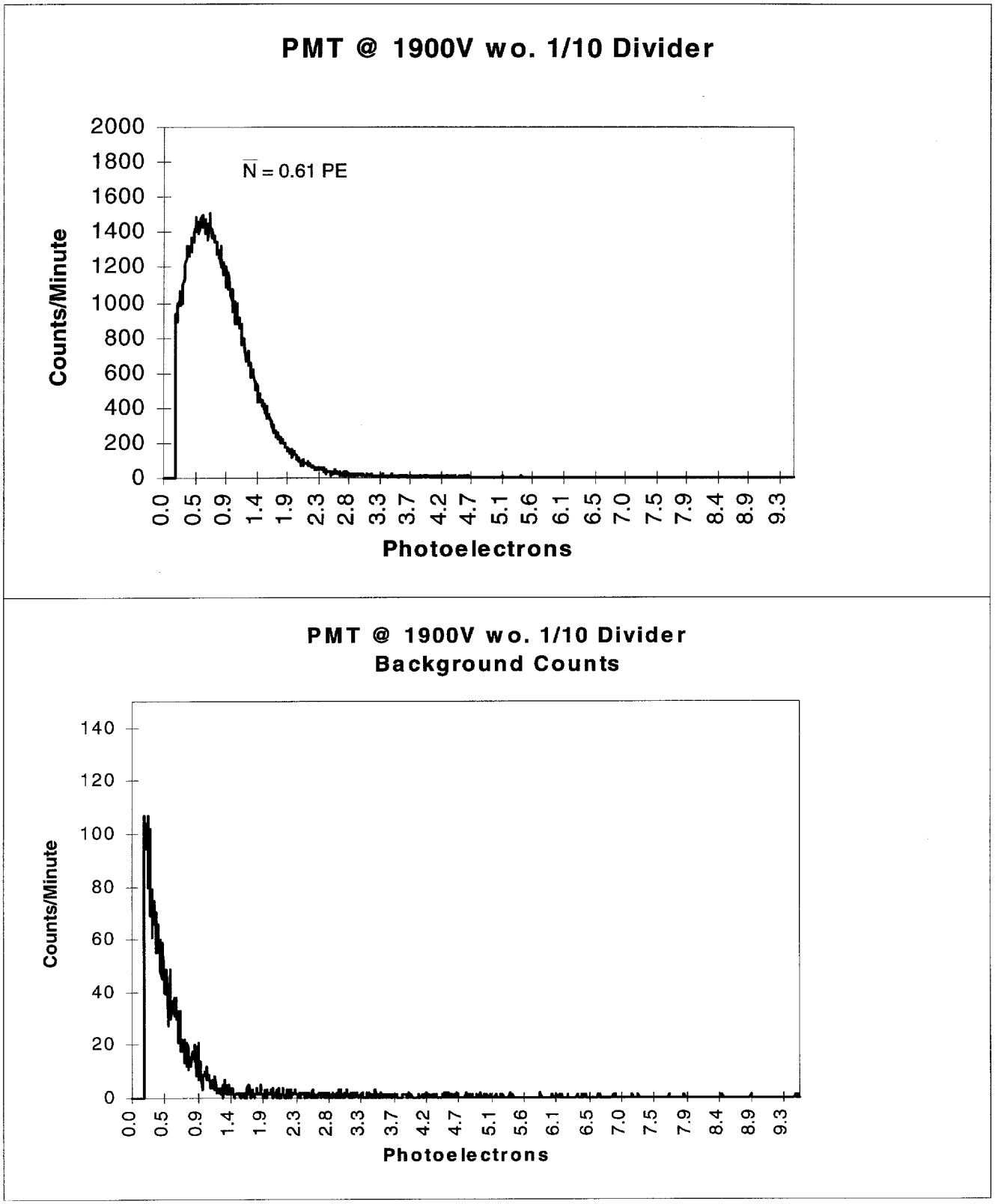

Figure 12: Pulse Height Spectra for the Teflon Diffuser in the Experimental Cell Using These Spectra are for the Kuraray Y11 Fiber

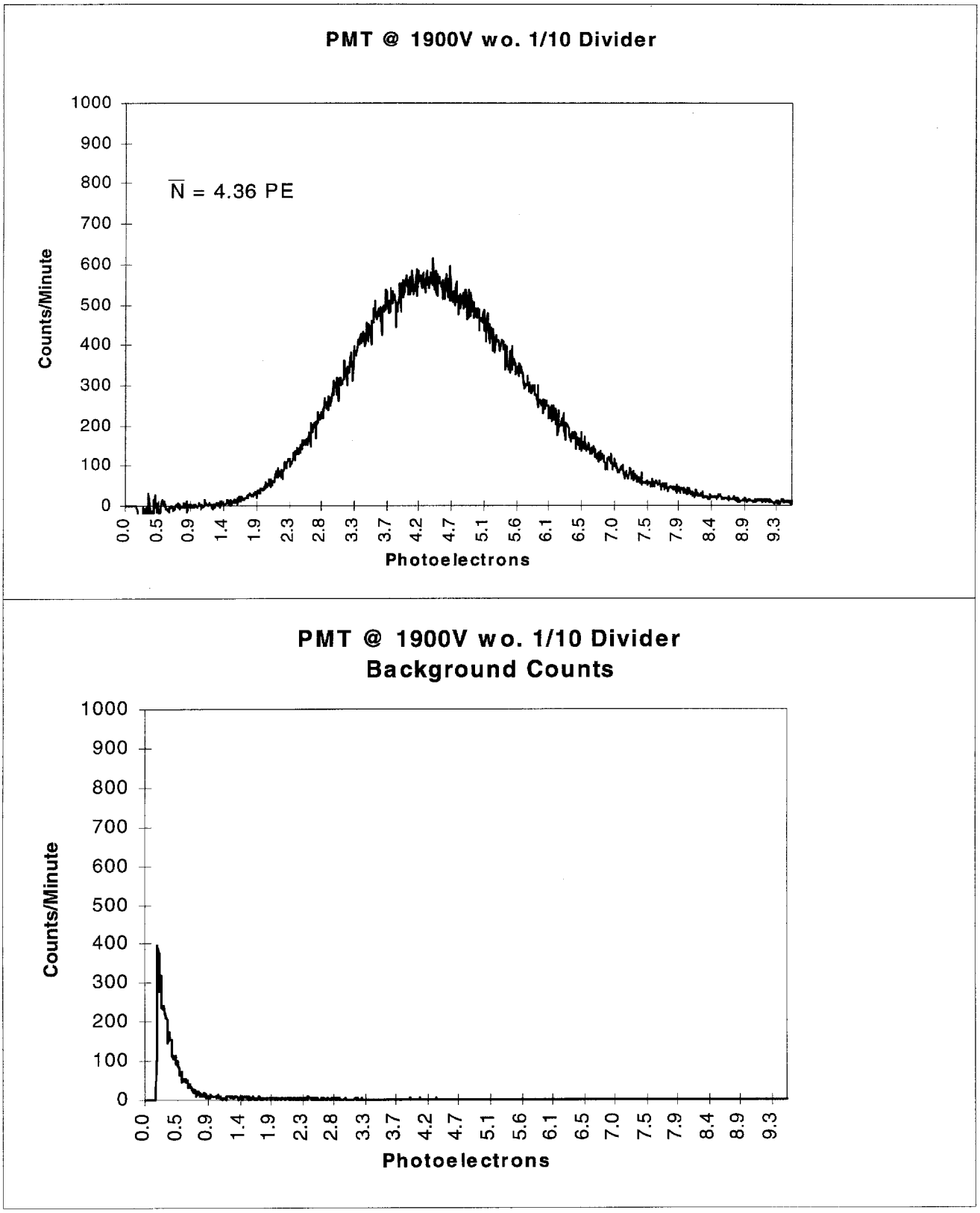

Figure 13: Pulse Height Spectra for the Teflon Diffuser in the Experimental Cell Using These Spectra are for the Pol.Hi.Tech S0048-100 Fiber

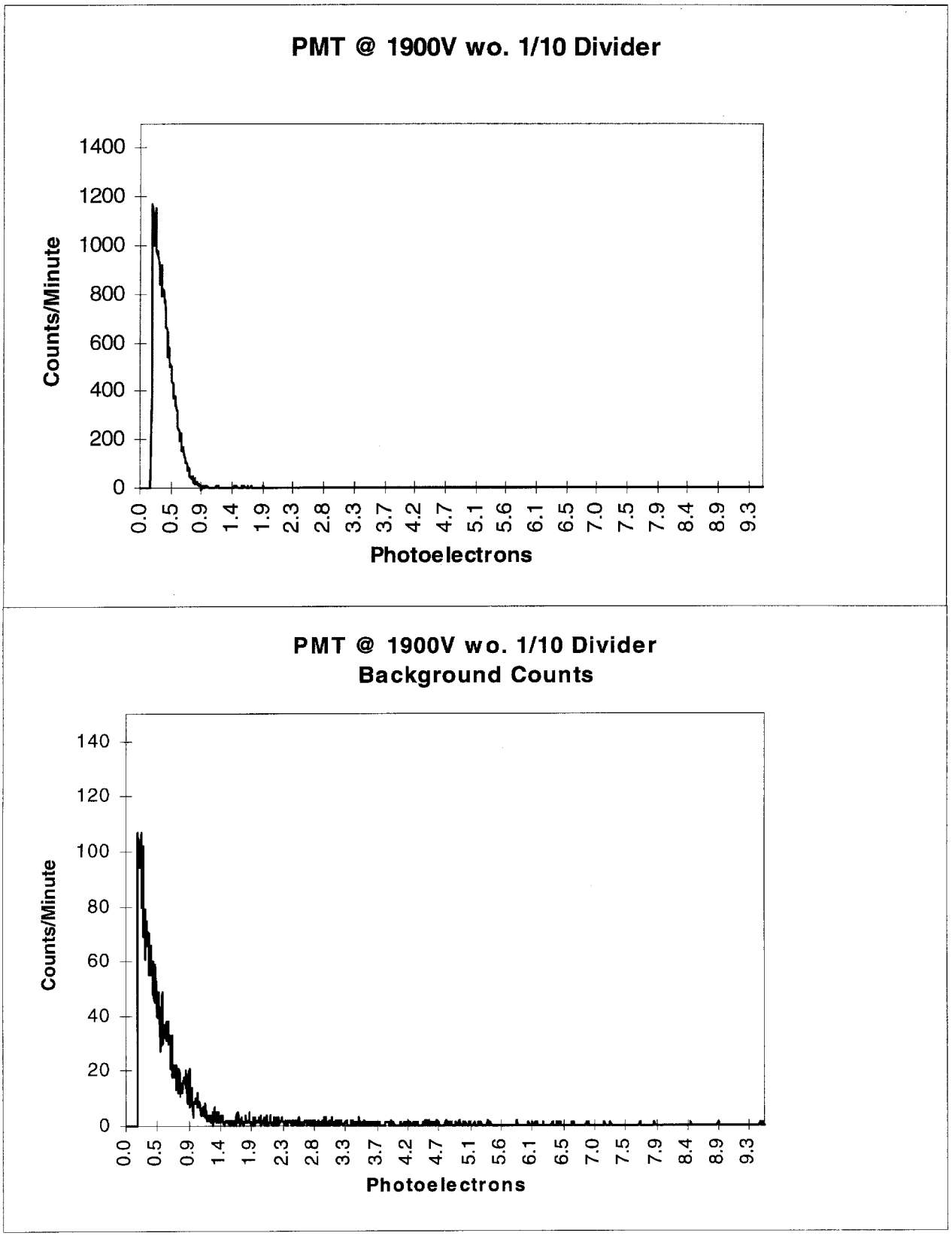

Figure 14: Pulse Height Spectra for the Alpha Source in the Experimental Cell
These Spectra are for the Kuraray Y11 Fiber

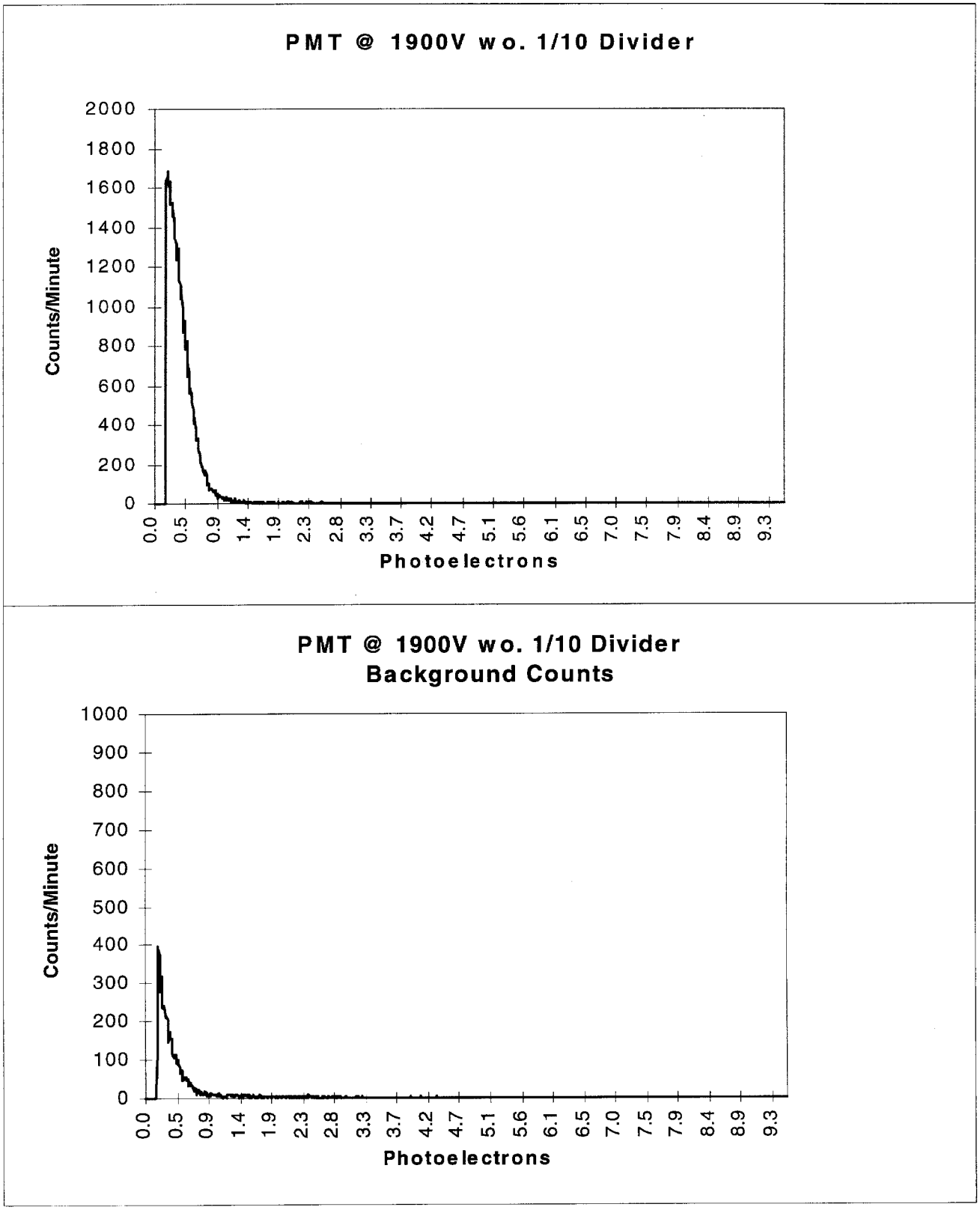

Figure 15: Pulse Height Spectra for the Alpha Source in the Experimental Cell
These Spectra are for the Pol.Hi.Tech S0048-100 Fiber

Chapter 5
Data Analysis

5.1 Overview

The overall goal of this section is to calculate the transport efficiency, cell efficiency, and XUV production rate described in the previous sections from the data in chapter 4. In terms of format, each calculation has two associated sections. The first section consists of the mathematics associated with the calculation. Given along with the quantity being measured is its associated error value. In the second section associated with a given measurement is an error section which details the procedure by which the error values in the first section are obtained.

Leading up to the efficiency measurements are a number of smaller calculations. First, the total output of the Teflon diffuser is calculated. Subsequently, the light output observed with the diffuser in the cell is presented. This completes all the calibration data. Next, the scintillation data is presented which is used to determine the number of XUV photons being generated. Finally, the XUV production is calculated from the decay properties of the source.

In the very last section, a minimum scintillation rate is discussed. The value is used to basically determine how many XUV are needed per alpha decay to obtain an observable signal. This information is very useful and is used in section VI to predict the performance of the present XUV detection system if applied in the actual UCN trapping experiment.

5.2 Teflon Diffuser Output

5.2.1 Analysis

The analysis given in this section focuses on determining the total light output from the Teflon diffuser. To accomplish this task, a number of steps need to be taken. The first part of the calculation involved determining the number of photoelectrons corresponding to the observed peak. Then, by using the quantum efficiency of the PMT and the throughput of the integrating sphere, the total output is obtained and its associated errors are calculated. In the section following, a detailed error analysis is given.

Since the signal observed represented a multiphotoelectron peak, the assumption is made that the distribution obtained is a Gaussian. If we postulate that there are “n” channels/photoelectron, the peak observed is a “Nn” photoelectron peak where “N” is the channel number corresponding to the peak. The width of the peak at half height is, by definition of the Gaussian, n times the square root of N. By setting up a pair of

simultaneous equations, it is determined. Having the number of photoelectrons corresponding to the observed peak, multiplying by the quantum efficiency of the PMT yields the number of photons per pulse incident on the photocathode. Values of the quantum efficiency and their associated errors are obtained from Burle Inc., manufacturers of the PMT used.

In order to find the number of photons being emitted from the diffuser in each pulse, it is necessary to calculate the fraction of light which leaves the integration sphere, otherwise known as the throughput which is given by the following formula:

$$T = \frac{A_e R}{[1 - R(1 - A_p)]}$$

where T is the throughput, R is the reflectance in the coating, A_e is the ratio of the area of the exit port divided by the total sphere are, and A_p is the ratio of all the ports divided by the total sphere area. In this setup, the area of the entrance port is very small (approximately 1mm diameter) since the fiber supplying light to the diffuser was passed through a piece of high reflectivity Teflon coated Gortex. The reflectivity of the integrating sphere coating is estimated at approximately 97%, as given by typical manufacturer specifications. Dividing the number of photons per pulse arriving at the PMT by the throughput gives the total radiation emanating from the diffuser per pulse. Summarized in table 1 are the values obtained for the output diffuser output for various PMT voltages. The output can be easily converted to conventional time units by factoring in the frequency of the signal generator pulses, but this is unnecessary since the pulse characteristics were not changed when placing the diffuser in the cryogenic setup.

		Total Diffuser Output				
PMT	Average	Output	Quantum	Throughput	Photons	Error
Voltage (V)	PE Count					
1900	87.0	450	0.23	0.11	3400	970
1800	68.4	450	0.23	0.11	2700	
1700	74.5	450	0.23	0.11	2944	
1600	84.0	450	0.23	0.11	3300	
1500	101.0	450	0.23	0.11	3900	
1400	74.5	450	0.23	0.11	2900	
Average Number of Photons/Pulse = 320						

Table 1: Total Diffuser Output

5.2.2 Errors

In characterizing the total luminescent output of the Teflon diffuser, two major errors enter into the calculation: the quantum efficiency of the PMT and the throughput of the integrating sphere. The total radiation per pulse (ϕ) is given by:

$$\phi = \frac{\mathrm{N}}{\mathrm{T}\eta}$$

where N is the number of photoelectrons per pulse, h is the quantum efficiency of the PMT at 450nm, and T is the throughput of the integrating sphere. The variance in the flux measurement is given by:

$$\sigma_{\phi}^{2} = \frac{\partial \phi}{\partial T}\sigma_{\mathrm{T}}^{2} + \frac{\partial \phi}{\partial \eta}\sigma_{\eta}^{2}$$

where σ_T^2 and σ_η^2 are the variances of the throughput and the quantum efficiency, respectively. Since these quantities in turn depend on the reflectivity of the integrating sphere and the spectral response of the PMT, the variance equation becomes:

$$\sigma_{\phi}^{2} = \left(\frac{\partial \phi}{\partial T}\frac{\partial T}{\partial R}\right)^{2}\sigma_{R}^{2} + \left(\frac{\partial \phi}{\partial \eta}\frac{\partial \eta}{\partial S}\right)^{2}\sigma_{S}^{2}$$

where σ_R^2 and σ_S^2 are the variances associated with the reflectivity and spectral response, respectively. According to the literature published by Melles-Griot [18], the standard deviation in the reflectivity of the 152mm sphere used in this experiment is 1%. In figure 16, the spectral response of the PMT is given as a function of wavelength [19]. From this graph, the deviation in the spectral response is approximated to be 4 mA/W. Substituting these uncertainties to the equation above yields a standard deviation of 970 photons/pulse in the measured total light output per Teflon diffuser pulse. In other words, the total diffuser output is accurate to about 30%. The errors generated by the width in the emission spectrum of the LED are ignored because the spectral response of the PMT is approximately linear in the 405-475nm range. Using the quantum efficiency associated with the peak output wavelength, 450nm, therefore introduces negligible error.

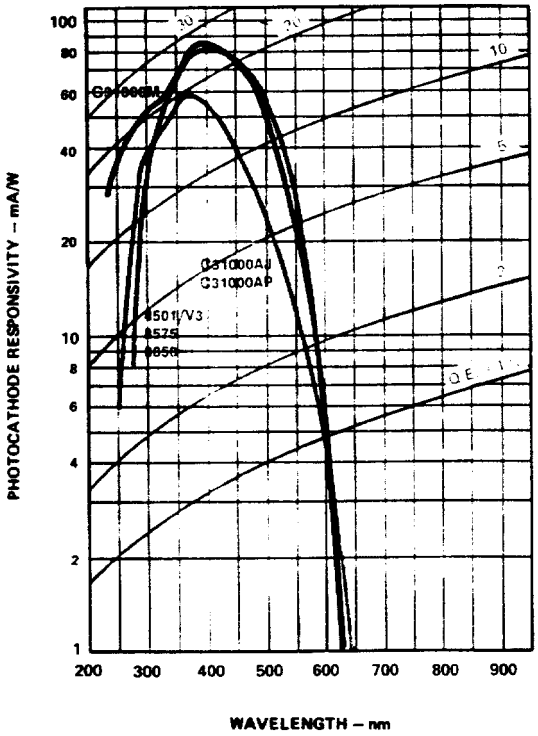

Figure 16: Spectral Response of PMT

5.3 Teflon Diffuser in the Cell & Transport Efficiency

5.3.1 Analysis

Here the primary focus is on calculating the number of photons that are observed exiting the cryogenic rig when the Teflon diffuser is in place and switched on. Using the calculations of the previous section, the number of photoelectrons observed is used to obtain the total photon count. The fiber transport efficiency and its uncertainty are presented in this section. Similar to the total diffuser output measurement, errors are discussed in 5.2.2.

It is assumed that the number of counts per photoelectron, n, is only a function of the amplifier gain and PMT voltage. As a result, running the cryogenic portion of the experiment with the same gain and voltage leaves n unchanged. Multiplying the number of photoelectrons per pulse by the quantum efficiency of the PMT again yields the number of photons incident on the photocathode. Dividing the photons detected from the fiber by the total diffuser output calculated in the previous section yields the transport efficiency of the WLS fiber. The transport efficiency is defined in this experiment as the ratio of the number of photons detected outside the cell to the total number emanating in the cell, and is some function of the inherent quantum efficiency of the fiber and the cell geometry. Provided in

table 2 are the values for both the S48 and Y11 fibers of the radiation leaving the WLS fiber and the transport efficiency of the fiber.

Transport Efficiency							
PMT Voltage(V)	WLS Fiber	Output λ (Peak) nm	Avgerage PE Count	Quantum Efficiency	Photons per	Transport	Error
1900	Y11	505 nm	0.61	0.12	5.08	0.158	0.05%
1900	S0048-100	480 nm	4.36	0.16	27.25	0.845	0.23%

Table 2: Diffuser Output in Experimental Cell and Transport Efficiency

5.3.2 Errors

The equation giving the observed light output (ϕ') when the diffuser is placed in the experimental is simply:

$$\phi' = \frac{N'}{\eta'}$$

where N' is the number of photoelectrons observed and ϕ' is the quantum efficiency of the PMT at the peak emission wavelength of the WLS fiber. The variance associated with the measurement is:

$$\sigma^2_{\phi'} = \left(\frac{\partial \phi' \ \partial \eta'}{\partial \eta' \ \partial S} \right)^2 \sigma^2_S$$

where the variance in the spectral response, is taken to be 16 mA/W as above. The standard deviation associated with the light observed through the WLS fiber when the Teflon diffuser is turned on in the cell is 0.42 photons/pulse (8.27%) when using the Y11 fiber, and 1.76 (6.45%) photons/pulse when using the S48 fiber.

As developed in section 5.3.1, the transport efficiency is the ratio of ϕ' to ϕ. The variance in the transport efficiency measurement is given by:

$$\sigma_{TE}^2 = \left(\frac{\partial TE}{\partial \phi}\right)^2 \sigma_{\phi}^2 + \left(\frac{\partial TE}{\partial \phi'}\right)^2 \sigma_{\phi'}^2$$

Using the values for the variances of the output values obtained in section 5.2.1, the standard deviation associated with the transport efficiency (TE) measurement is 0.050% (32% of TE) for the Y11 fiber and 0.23% (27% of TE) for the S48 fiber.

5.4 Scintillation Data

5.4.1 Analysis

In this section, the number of photons observed by PMT when the alpha source is in place is determined. There is a calculation difference in these runs in comparison to the previous photon counting scheme. In these runs, since an entire single photoelectron peak was not observed, the integral of the number of counts must be studied. The cell efficiency and its associated uncertainty are also calculated as well in this section. Errors are presented in 5.4.2.

During this phase of the experiment, the Teflon diffuser is still in the cell, but no light is being sent to it. As a result, the geometry of the cell does not change from the calibration runs to the data runs. By comparing the data to the background spectra taken, it seems fairly clear that peak observed is a single photoelectron peak. In the background spectrum, there are three major components. At very small pulse heights there is high number of counts which generally corresponds to electrical noise. Larger pulse heights generally correspond to the one photoelectron peak generated by the thermionic emission of electrons in the PMT. At very large pulse height values there are some counts due to cosmic rays and radioactive particles present in the testing environment. Since the peak in the data spectrum is located at the same pulse height as the dark current signal identified in the background, it must be a single photoelectron peak. It is necessary, however, in this instance to integrate the number of counts over the whole peak since its apex is not visible. As a consequence, the background counts are subtracted before taking the integral. Dividing the number of counts observed by 60 seconds, the length of the run, yields the number of photoelectrons generated per second, which is then converted to photons via the quantum efficiency.

Having previously calculated the transport efficiency of the WLS fibers, it is possible to calculate the number of blue photons generated by the TPB in the cell by simply dividing the flux detected by the PMT by the transport efficiency. To determine the number

of XUV photons present we assume that the fluorescence efficiency of the TPB is 100%. Combining these calculations gives us the cell efficiency (CE), the ratio of photons observed to XUV photons produced, as shown in table 3. The CE is useful in determining the threshold XUV production rate which can be detected.

Cell Efficiency

PMT Voltage (V)	WLS Fiber	Single PE Counts	Photons per Sec	Blue Photons per Sec	XUV Photons per Sec	Cell Efficiency %	Error
1900	Y11	29,400/min	4083.33	2.59E+06	2.59E+06	0.16	0.52%
1900		54,400/min	5666.67	6.70E+05	6.70E+05	0.85	0.28%

Table 3: Cell Efficiency

5.4.2 Errors

By simple calculation, the cell efficiency is equal to the product of the transport efficiency and the fluorescence efficiency of the TPB. The variance in the CE is thus given by:

$$\sigma_{CE}^2 = \left(\frac{\partial CE}{\partial TE}\right)^2 \sigma_{TE}^2 + \left(\frac{\partial CE}{\partial FE}\right)^2 \sigma_{FE}^2$$

where σ_{TE}^2 and σ_{FE}^2 are the variances associated with the TE and FE. On the basis of measurements made by [6], the FE measurement has a standard deviation of 0.1. As a result, the CE has a standard deviation of 0.052% (33% of the CE) when the cell consists of the Y11 WLS fiber and 0.28% (33% of the TE) when using the S48 fiber. The errors associated with the slightly different peak emissions of the LED and TPB are not considered here. The emission FWHMs for both TPB and the LED are 70nm and the maximum output wavelength differs by only 10nm. Errors associated with the throughput and PMT quantum efficiency are of greater significance.

From the error analysis given in the previous section, it is clear that the greatest error in the cell efficiency measurement comes from the uncertainty associated with the throughput of the integrating sphere. The throughput, very sensitive to the value of the reflectivity of the sphere surface, directly affects the total photon count per pulse, and by simple extension, the transport efficiency. Measuring the reflectivity of the integrating sphere coating is difficult to carry out precisely and was not attempted. Melles-Griot did

not have any specific measurements of the reflectivity either. Such being the case, attempts at improving the accuracy of the cell efficiency were not made.

5.5 Alpha-Helium Collisions

5.5.1 Analysis

It is easy to determine, using the previous determinations CE, the number of XUV photons produced per alpha collision. It is useful to know the decay rate of the alpha source. The source has a half-life of 138 days, and was measured to have a total decay rate of 3000cts/sec 210 days prior to

XUV Production						
WLS Fiber	XUV Photons per Sec	Decays per Sec	Energy (MeV)	XUV Photons per Decay	XUV Photons per keV	Error
Y11	2.59E+06	1040	5.3	2490.15	0.47	0.18
S0048-100	6.70E+05	1040	5.3	644.64	0.12	0.45

Table 4: XUV Production

taking the data given above. The fraction of sample present at the time of the experiment is given by the following:

$$\frac{N(t)}{N(0)} = e^{\frac{-\ln 2(t)}{t_h}}$$

where N represents the number of radioactive atoms, t the time, and t_h the half-life. Being proportional to the amount of radioactive material present, the decay rate at the time of the experiment is calculated from the above equation. Dividing the number of XUV photons by the decay rate gives the number of ultraviolet photons released per decay event. Alpha particles produced from Polonium are 5.3 MeV in energy. Table 4 gives the number of XUV photons per keV (n) of incident energy for alpha particles.

5.5.2 Errors

There are a number of uncertainties associated with n, the number of XUV photons emitted per keV of bombarding alpha particles. By definition, n is equal to:

$$n = \frac{I_{xuv}}{I_{\alpha}}\left(\frac{1}{5300}\right)$$

where I_{xuv} is the XUV intensity and I_{α} is the alpha particle intensity. The XUV intensity is deduced from the PMT signal observed with the radioactive source in place and the cell efficiency. The XUV intensity and its associated variance are given by:

$$I_{xuv} = \left(\frac{N'' Int}{60\eta'}\right)\left(\frac{1}{CE}\right)$$

$$\sigma^2_{I_{XUV}} = \left(\frac{\partial I_{xuv}}{\partial \eta'}\right)^2 \sigma^2_{\eta'} + \left(\frac{\partial I_{xuv}}{\partial CE}\right)^2 \sigma^2_{CE}$$

where N'' is the number of photoelectrons observed and Int is the total number of counts. The errors associated with the quantum efficiency have already been calculated for both the WLS fibers. The intensity of the alpha source is, in this particular case, simply the intensity measured at a given time multiplied by a decay factor which takes into account the natural radioactive decay of the alpha source. The variance of the alpha particle intensity is simply then:

$$\sigma^2_{I_{\alpha}} = \left(\frac{\partial I_{\alpha}}{\partial C}\right)^2 \sigma^2_C$$

where C is the original decay rate measurement and σ^2_C is its associated variance. Combing the above equations gives the following expression for the variance of n.

$$\sigma_n^2 = \left(\frac{\partial n}{\partial I_{xuv}}\right)^2 \left[\left(\frac{\partial I_{xuv}}{\partial \eta'}\right)^2 \sigma_{\eta'}^2 + \left(\frac{\partial I_{xuv}}{\partial CE}\right)^2 \sigma_{CE}^2\right] + \left(\frac{\partial n}{\partial I_\alpha}\frac{\partial I_\alpha}{\partial C}\right)^2 \sigma_C^2$$

The greatest contribution to the overall uncertainty in n comes from the uncertainty in the measured decay rate of the alpha source. The alpha source was used by [15] in various experiments after the rate was measured before being used in this experiment. Though it is unlikely that flaking occurred in this experiment, no information about source degradation prior to the commencement of the current work is available. Such being the case, it is assumed that some flaking did occur due to usage and the standard deviation of the intensity measurement is approximated as 500 counts/sec. This gives a standard deviation of 0.18 XUV photons/keV associated with n using the Y11 data, and 0.045 XUV photons/keV using the S48. The two measurements made for the scintillation rate are agreement within two standard deviations.

It is important to note, however, that these measurements are discrepant from those obtained by Stockton [19] in his electron bombardment experiment. Stockton estimates a value of 4 XUV photons per keV assuming an absolute quantum efficiency of 100% for sodium salicylate. Later investigations of sodium salicylate [6] have demonstrated the actual value to be approximately 41%. In light of this information, Stockton's data would indicate a XUV production rate of approximately 8 XUV photons per keV. Some factors which might result in the lower value obtained in this experiment are given here.

For one, it is possible that TPB was dirty. Having been kept on the shelf for some time and handled by a few different hands, dust and oil might have accumulated on the surface. These particles, if present, would absorb the XUV photons produced in the helium and thus reduce the calculated value of n. It is also possible that while moving the alpha source into and out of the cell, some TPB flaked off, this producing the same effect in n. Finally, another possible problem lies with the quantum efficiency of the WLS fiber. Hitherto it had been assumed that the fiber absorbs and wave shifts equally at the emission wavelength of TPB (440 nm) and that of the LED (450nm). If the spectral response is varied, the transport efficiency measurements would change and thus the number of XUV photons being produced would change. Some combination of all these factors might be involved in the discrepant value n. Many of these errors could be eliminated with further experimentation.

5.6 Minimum Scintillation Rate

After having calculated the cell efficiency, it is possible to estimate how many XUV photons should be produced per decay event in order to observe a signal. In this context, observing a signal means obtaining a single photoelectron for every decay event. Using the calculations in section 4.3, approximately 52.1 XUV photons would have to produced per decay in a setup employing the Y11 fiber to get a photoelectron. Similarly, 7.35 XUV photons per decay event would be needed when using a S48 fiber. This difference in the number of required XUV photons reflects the differences in transport efficiency of the fibers and the variation in quantum efficiency of the PMT at different wavelengths.

Chapter 6
Conclusion

The data acquired from this experiment are used here to make predictions on the operating parameters of the XUV down-converting cell currently being developed by the Doyle Group. There are two major geometrical effects which have to be considered when applying the measurements obtained here to the actual cell in the neutron experiment: cell length and diameter. The length of the cell is important because of the attenuation present in the WLS fibers. The transport efficiency is proportional to the attenuation which is given by:

$$e^{-\frac{L}{L_a}}$$

where L is the length of the fiber used and L_a is the attenuation length. In the present experiment, a 1.2 meter strand of fiber was used, where as in the neutron experiment 1.5 to 2.0 meter segments will be used. Hence a single fiber in the actual cell will have a lower transport efficiency by approximately 15%.

In addition to length, the diameter of the cell is also crucial in determining the cell efficiency. Using simple optical calculations, the percentage of blue photons that get into the WLS fiber is given by:

$$R^{\frac{\pi d_t}{d_f}}$$

where d_f is the diameter of the fiber, d_t is the diameter of the tube, and R is the reflectivity of the cell wall. Though, the reflectivity is not known at present for TPB evaporated onto Gortex, 90% is a reasonable approximation to use in these rough calculations. The actual cell is going to be 1.5" in diameter. Therefore, in a single fiber, the cell efficiency will be decreased by a factor of approximately 4600.

If a cell is constructed with a single fiber uncoiled, after adjusting for the change in efficiency, is approximately, the number of XUV photons needed to obtain a single photoelectron is 240,000 using the Y11 and 33,800 S48. According to the calculations [1], 3000 XUV photons are expected to be released per neutron decay. In this geometry, it is probably not possible to detected individual decays.

Of course, there are methods by which the detection efficiency can be improved in a larger cell. For one, if the fibers are coiled, a much larger percentage of the blue photons

emitted by the TPB can be captured. In addition, the use of VLPCs can improve the XUV detection system. Lets redo the calculation for a coiled fiber. Assume that we keep the ratio of the TPB covered area to the area of the fibers at the same value present in this experiment. Such being the case, the area of the TPB layer in the actual cell is 9 times that of small experimental cell (the actual cell being approximately 3 times longer and wider). Therefore, the area of the fibers must be 9 times larger as well. Being simply proportional to the fiber length, a nine-fold increase in area translates into a nine-fold increase in length if the fibers are placed against the surface of the TPB. Since the circumference of the actual cell is ~4.71 in, the fiber can be coiled approximately three times in the cell. Three coils decreases the cell transport efficiency by an addition 4% due to attenuation effects. The values yield the number of XUV photons per decay to yield a single photoelectron as being 62.5 for the Y11 fiber and 8.82 for the S48. Given that each neutron generated 3000 XUV photons per decay, there should be 48 photoelectrons per decay using the Y11 fiber and 340 photoelectrons for the S48 fiber. It must be kept in mind, however, that these values are based on a 90% cell reflectivity. If the actual reflectivity is lower, as it might be, the number of photoelectrons produced per decay would be much less, though, in all probability, still detectable.

References

[1] J.M. Doyle. Determination of the neutron lifetime using magnetically trapped neutrons. *NSF Grant Proposal*, 1994.

[2] J.M. Doyle and S.K. Lamoreaux. On measuring the neutron beta-decay lifetime using ultra-cold neutrons produced and stored in a superfluid 4He filled magnetic trap. *Europhysics letters*, 26(4):253-258, 1994.

[3] Lally et al. UV quantum efficiencies of organic fluors. *Nuclear Instruments and Methods in Physics Research B*. 117:421-427,1996.

[4] D.N. McKinsey et al. Fluorescence Efficiencies of Thin Scintillating Films in the Extreme Ultraviolet Spectral Region. Submitted for publication. .

[5] E.C. Bruner. *Jr. J. Optical Society of America*. 59:204,1969.

[6] Garolite was purchased from *McMaster-Carr, Inc*.

[7] Stycast 2850 is Manufactured by *Emerson Cummings, Inc*.

[8] Castolite AC Clear Casting Plastic (Polystyrene) is Manufactured by *AIN Plastics*.

[9] *Pol.Hi.Tech Detector Catalogue*.

[10] M. Chung and S. Margulies. Effects of Stress and Strain on Scintillating and Clear Fibers. *IEEE Transactions on Nuclear Science*. 42(4):323-327,1995.

[11] M. Adams et al. A Detailed Study of Plastic Scintillating Strips with Axial Wavelength Shifting Fiber and VLPC Readout. *Submitted to Nuclear Instruments and Methods in Physics, Section A*.

[12] R. Wojcik et al. Embedded waveshifting fiber readout of long scintillators. *Nuclear Intruments and Methods in Physics Research A*. 342:416-435,1994.

[13] R. Golub. *HMI, Berlin*. Private Communication.

[14] Clear Optical Fiber Manufactured by *Edmund Scientific*.

[15] High Brightness LED Manufactured by *Panasonic*, Purchased from Digi-Key

[16] *Burle Photomultiplier Handbook*, 1987.

[17] PMT Housing Manufactured by *Products for Research*.

[18] *Melles-Griot Catalogue*

[19] M. Stockton, et al. Ultraviolet Emission Spectrum of Electron-Bombarded Superfluid Helium. *Physics Review Letters*. 24(12):654-657, 1970.